Retraction for *Journal of Materials Chemistry B*:

Hydrophilic hybrid materials with magnetism & NIR fluorescence *via* surface-initiated RAFT polymerization

Weiwei He, Lifen Zhang, Bing Han, Liang Cheng, Nianchen Zhou, Zhuang Liu and Zhenping Cheng

J. Mater. Chem. B, 2013, **1** (26), 3257–3266 (DOI: 10.1039/c3tb20262c). **Retraction published 24 September 2013**

We, the named authors, hereby wholly retract this *Journal of Materials Chemistry B* article due to the subsequent realisation that fluorescence measurements reported in the article should have been measured through a long-pass filter. The emission at 750 nm reported from the excitation of the monomer 1-(4-vinyl benzyl)-2-naphthyl-benzimidazole by UV light, is actually a second order diffraction artefact of the 380 nm emission. The claim that the monomer is capable of emitting near infrared fluorescence under UV light excitation in the article is false.

Signed: Weiwei He, Lifen Zhang, Bing Han, Liang Cheng, Nianchen Zhou, Zhuang Liu and Zhenping Cheng, September 2013

Retraction endorsed by Liz Dunn, Managing Editor, *Journal of Materials Chemistry B*

Journal of Materials Chemistry B

RSC Publishing

PAPER

Hydrophilic hybrid materials with magnetism & NIR fluorescence *via* surface-initiated RAFT polymerization

Cite this: *J. Mater. Chem. B*, 2013, **1**, 3257

Weiwei He,[a] Lifen Zhang,[a] Bing Han,[a] Liang Cheng,*[b] Nianchen Zhou,[a] Zhuang Liu[b] and Zhenping Cheng*[a]

Received 22nd February 2013
Accepted 25th April 2013

DOI: 10.1039/c3tb20262c

www.rsc.org/MaterialsB

In the current work, one monomer (denoted as M_{HB}) capable of emitting near infrared (NIR) fluorescence under UV light excitation is prepared and employed to perform (co)polymerization with a commercial hydrophilic and biocompatible monomer, poly(ethylene glycol) monomethyl ether methacrylate (PEGMA), on the surface of silica coated iron oxide nanoparticles (NPs). PEGMA is used to either copolymerize or chain-extend M_{HB} after polymerization to improve the hydrophilicity of the NPs which is essential for practical application in bio-related areas. The as-prepared NPs in different surface modification steps were investigated by Fourier transfer infrared (FT-IR), thermogravimetric analysis (TGA), transmission electron microscope (TEM) and UV-vis spectroscopic techniques. The crystal form of the NPs was checked by powder X-ray diffraction (XRD) and it showed that the magnetic core is made up of ferroferric oxide. The magnetic properties of the NPs were measured by vibrating-sample magnetometer (VSM) and all NPs exhibited superparamagnetism. The final NPs possessing magnetic and NIR fluorescent properties have potential applications in biological areas as dual-model imaging agents, and their application as contrast agents for magnetic resonance imaging (MRI) is investigated.

Introduction

Magnetic iron oxide has drawn a great deal of attention due to its promising and practical applications in a wide range of areas, one of which, particularly for superparamagnetic compounds, is as magnetic resonance imaging (MRI) contrast agents for tumor diagnosis.[1–13] Recently, nanoparticles (NPs) of magnetic iron oxide combining fluorophore, as called "two in one" NPs, have been the focus of research worldwide due to their remarkable characteristics and promising perspectives in biological areas and, to date, several methods have been developed successfully to prepare it.[14–25] *In vivo* detection methods such as fluorescence imaging and MRI, two complementary techniques, can be performed simultaneously with such NPs,[26–31] which would provide much more comprehensive information about the situation and state of the patients and therefore facilitate detection of tumors or cancers *via* the "two in one" NPs at an early stage. So far, most of the reported bifunctional NPs with magnetism and fluorescence emit light in the UV-vis range and are based on inorganic compounds, such as quantum dots (QDs), which are usually toxic. Developing new approaches to fabricate biocompatible bifunctional NPs with magnetism and fluorescence is appealing and urgent. Driven by such a force, our group has also been engaged in developing new strategies to prepare such preferable bifunctional NPs taking advantage of controlled radical polymerization techniques and less toxic organic chromophores. Polymer sequences, which might affect the physical properties as a result of alternating the photo-physical features of the as-prepared materials, can be facilely achieved through living radical polymerization. To date a few successful cases have already been reported by our group.[18,19]

In fact the organisms themselves usually generate fluorescence in a certain range of wavelengths automatically or under an external irradiation, which brings in background interference when performing *in vivo* imaging, an obstacle to the acquisition of exact information thus reducing the accuracy of detection.[32,33] Fortunately, there exists a spectrum window between 650 and 900 nm which overlaps with the NIR region (700–900 nm), where the background emission fluorescence of the object itself could be greatly minimized or even completely eliminated in some cases.[34–36] Therefore, NIR fluorophores are so appealing that so far a number of NIR emitting species, mainly including quantum dots (QDs)[37] and organic dyes,[38–40] were successfully synthesized and some of them or their derivatives have been successfully applied for *in vivo* imaging or bio-labeling. Accordingly, magnetic NPs with NIR fluorescence, a new generation of dual modal imaging agents, are more and more attractive for researchers. As is well known, QDs generally

[a]*Jiangsu Key Laboratory of Advanced Functional Polymer Design and Application, Department of Polymer Science and Engineering, College of Chemistry, Chemical Engineering and Materials Science, Soochow University, Suzhou 215123, China. E-mail: chengzhenping@suda.edu.cn*

[b]*Functional Nano and Soft Materials Laboratory (FUNSOM), Jiangsu Key Laboratory for Carbon-Based Functional Materials and Devices, Soochow University, Suzhou 215123, China. E-mail: lcheng2@suda.edu.cn*

consist of heavy metals and are usually seriously toxic to human beings and other living species. In most reported cases QDs are wrapped in an inert shell such as silica when preparing such "two in one" NPs. Although this renders them much more stable than naked NPs and keeps them isolated from the surroundings, leakage of the heavy metal, when being administered in the body, is still the main concern which might trigger serious safety issues. On the other hand, organic dyes are much less toxic and their diversity can also meet various demands.[41–46] Despite their many advantages, while they have been widely investigated separately, surprisingly combinations of NIR dyes with magnetic NPs in one unit are less available.

Herein we report a facile strategy to prepare such "two in one" NPs with superparamagnetism and NIR fluorescence by surface-initiated reversible addition–fragmentation chain transfer (SI-RAFT) technique. One NIR dye monomer (denoted as M_{HB}) capable of emitting NIR fluorescence was used to perform (co)polymerization with a commercial hydrophilic and biocompatible monomer, PEGMA, on the surface of silica coated iron oxide NPs. Silica coated iron oxide was selected as the magnetic core for its unique advantages such as improving the colloidal stability and preventing fluorescence quenching of the dyes from the magnetic iron oxide core.[14] Besides, PEGMA is employed to perform the copolymerization or chain-extension on the surface of NPs to increase the hydrophilicity and biocompatibility of the resulting NPs.

Experimental section

Materials

Poly(ethylene glycol) monomethyl ether methacrylate (PEGMA) (M_n = 475 g mol^{-1} or 1100 g mol^{-1}) (>99%), was purchased from Aldrich. It was purified by passing through a column filled with neutral aluminum oxide and stored at −18 °C before use. Tetraethoxysilane (TEOS) (>98%, Fluka) and (*p*-chloromethyl) phenyl trimethoxysilane (95%, ABCR) were used as received. *N*,*N*-dimethyl formamide (DMF, analytical reagent) was obtained from Shanghai Chemical Reagents Co. and dried with an activated molecular sieve (4 Å). Toluene (analytical reagent) was purchased from Shanghai Chemical Reagents Co. and was dried by distillation with sodium. Ferric chloride hexahydrate ($FeCl_3 \cdot 6H_2O$) (>99%), ferrous sulfate ($FeSO_4 \cdot 7H_2O$) (>99%), citrate acid (>99%), potassium hydroxide (KOH), ammonia ($NH_3 \cdot H_2O$, 25%), ethanol, acetone, cyclohexanone and all other chemicals were obtained from Shanghai Chemical Reagents Co. and were used as received unless mentioned.

Synthesis of magnetic NPs (Fe_3O_4)

The colloidal magnetic NPs modified by citric acid were prepared by a chemical coprecipitation method and dispersed *in situ* in water as a ferrofluid. The procedure was as follows: $FeCl_3 \cdot 6H_2O$ (4.1 g, 0.015 mol) and $FeSO_4 \cdot 7H_2O$ (2.35 g, 0.08 mol) were added to 100 mL of deionized water in a three-neck flask under a flow of Ar. 25 mL of $NH_3 \cdot H_2O$ (25%) were added to the flask after vigorous mechanical stirring for 0.5 h. Then a black precipitate formed quickly, and stirring was continued for 0.5 h. The product was collected and then redispersed into 100 mL of deionized water with 0.5 mL of citric acid (0.01 M), stirring for 15 min. The final product was collected from the suspension by centrifugation and washed with distilled water until pH = 7.

Synthesis of silica coated iron oxide (Fe_3O_4@SiO_2)

25 mL of TEOS were added to a mixture of 15 mL of $NH_3 \cdot H_2O$ (25%), 235 mL of H_2O, 750 mL of ethanol, and the previously washed Fe_3O_4 under mechanical stirring for 16 h under Ar. The NPs were isolated by centrifugation at 15 000 rpm. After discarding the supernatant, the sediments were redispersed in ethanol and centrifuged again. This purification cycle was repeated for four times and the product was dried under vacuum at room temperature for 24 h.

Synthesis of chloromethyl phenyl functionalized colloidal magnetic silica NPs (Fe_3O_4@SiO_2–Cl)

Typically, 1 g of dried Fe_3O_4@SiO_2 was dispersed in 40 mL of freshly distilled toluene with the aid of sonication, and 1 mL of (*p*-chloromethyl)phenyl trimethoxysilane was added after removing air by flushing with Ar for 30 min, then the flask was immersed in an oil bath at 90 °C. The mixture was stirred for 16 h, and then the solution was cooled and exposed to air. The NPs were washed under ultrasonication with abundant toluene and acetone in turn, collected by centrifugation and dried under vacuum at room temperature for 24 h.

Synthesis of RAFT agent-functionalized colloidal magnetic silica NPs (Fe_3O_4@SiO_2–BCBD)

The Fe_3O_4@SiO_2–BCBD NPs were prepared by the following procedure: a suspension of KOH (0.26 g, 0.004 mol) in DMSO (20 mL) was prepared, and carbazole (0.78 g, 0.004 mol) was added under vigorous stirring. The solution was stirred for 2 h at room temperature and then CS_2 (0.4 mL, 0.006 mol) was added dropwise. The resultant reddish solution was stirred for 12 h at room temperature, and then the prepared Fe_3O_4@SiO_2–Cl (0.80 g) was added. The mixture was stirred for further 36 h at room temperature. The NPs were recovered by centrifugation at 12 000 rpm for 15 min. The Fe_3O_4@SiO_2–BCBD NPs were washed under ultrasonication with abundant ethanol–H_2O (v/v = 1/1) solution and acetone for several times, precipitated by centrifugation and dried under vacuum at room temperature for 24 h.

Synthesis of monomer M_{HB}

Firstly, 1,2-diaminobenzene (2.21 g, 0.020 mol), 2-naphthoic acid (5.44 g, 0.032 mol) and polyphosphoric acid (1.12 g, 0.003 mol) were mixed and put in an oil bath at 180 °C under continuous vacuum for 30 min. After cooling down, the crude product was dissolved in DMSO and precipitated in deionized water and filtered. The product was dispersed in water and the suspension was adjusted at pH = 4–5, filtered and redispersed in water regulating the pH = 8–10 with NaOH. The intermediate product VNBI was dried in vacuum after filtration and purified

by recrystallization with ethanol. Separately, potassium carbonate (0.64 g, 4.6 mmol) was dispersed in DMF (140 mL) at 80 °C under stirring for 10 min. A solution of VNBI (1.08 g, 4.4 mmol) in DMF (60 mL) was added dropwise. After cooling down to 40 °C, 4-(chloromethyl)styrene (1.04 mL, 7.4 mmol) was added and the mixture was stirred for another 48 h. The resulting mixture was poured in 300 mL of deionized water, and extracted with ethyl acetate. The final product M_{HB} was obtained by concentrating and then purifying *via* column chromatography.

Grafting of M_{HB} shell from RAFT agent-functionalized Fe_3O_4@SiO_2–BCBD

General procedure for (co)polymerization of M_{HB} is as follows: M_{HB} (0.127 g, 0.35 mmol), Fe_3O_4@SiO_2–BCBD (50 mg), AIBN (0.38 mg, 2.3×10^{-2} mmol) and DMF (3 mL) were added in a dry ampoule and treated in ultrasonic for 5 min ($PEGMA_{475}$ (0.31 mL, 0.70 mmol) was added for copolymerization). The contents were purged with Ar for 10 min to eliminate the dissolved oxygen, and then the ampoule was flame-sealed. The polymerization proceeded in an oil bath held by a thermostat at the desired temperature (70 °C). After desired polymerization time, the ampoule was cooled by immersing it into iced water, and then, the reaction mixture was diluted by THF and centrifuged (1.2×10^4 r min^{-1}). This cycle of centrifugation and redispersion in THF was repeated four times to make sure that the free polymers were removed completely. The obtained Fe_3O_4@SiO_2@(co)polymer NPs was dried in vacuum oven at room temperature.

Block copolymerization of PEGMA using Fe_3O_4@SiO_2@PM_{HB} NPs as macro-RAFT agent

Fe_3O_4@SiO_2@PM_{HB} NPs (50 mg), PEGMA (0.31 mL, 0.70 mmol), AIBN (0.38 mg, 2.3×10^{-2} mmol) and DMF (3 mL) were added in a dry ampoule and treated in ultrasonic for 5 min. The content was purged with Ar for 10 min to eliminate the dissolved oxygen, and then the ampoule was flame-sealed. The polymerization proceeded in an oil bath held at the desired temperature by a thermostat (70 °C). After the polymerization time, the ampoule was cooled by immersing it into ice water, and then the reaction mixture was diluted by THF and centrifuged (1.2×10^4 r min^{-1}) to separate the free polymers. This cycle of centrifugation and redispersion in THF was repeated five times to make sure that the free polymers were removed completely. The final product, Fe_3O_4@SiO_2@PM_{HB}-*b*-PPEGMA NPs, was dried in a vacuum oven at room temperature.

Cleavage of the grafted polymers from the Fe_3O_4@SiO_2@PM_{HB}-*co*-PPEGMA NPs

Cleavage of the PM_{HB}-*co*-PPEGMA from the Fe_3O_4@SiO_2@PM_{HB}-*co*-PPEGMA NPs was carried out according to the procedure described in ref. 47. In a PTFE beaker, the PM_{HB}-*co*-PPEGMA grafted hybrid NPs (50 mg) was dispersed in 8 mL of THF. Then aqueous HF (48 wt%, 0.3 mL) was added and the reaction mixture was stirred at room temperature for 10 h. The resulting polymer was precipitated by pouring the polymer solution into a 20-fold excess of hexane, and then the precipitate was collected and dried in a vacuum oven at 30 °C overnight. The recovered PM_{HB}-*co*-PPEGMA was then subjected to ^{1}H NMR analysis.

HeLa cells culture and MR imaging

HeLa cells were cultured in Dulbecco's modified eagle medium (DMEM) containing 10% fetal bovine serum (FBS), streptomycin (100 U mL^{-1}) penicillin (100 U mL^{-1}), and 4 mM L-glutamine at 37 °C in a humidified 5% CO_2-containing atmosphere. For cellular imaging, cells were incubated with Fe_3O_4@SiO_2@(PM_{HB}-*co*-PPEGMA) NPs overnight. The cells were washed with PBS, centrifuged and then covered with agarose solution before MR imaging. The treated cells were scanned under a 3-T clinical MRI.

Cytotoxicity assay by MTT

The MTT assay was performed to evaluate the impact of Fe_3O_4@SiO_2@PM_{HB}-*co*-PPEGMA NPs on the viability of HeLa cells. The cells were seeded onto 96-well plates at a density of 1×10^4 cells per well for 24 h. Afterwards a series of concentrations of Fe_3O_4@SiO_2@PM_{HB}-*co*-PPEGMA NPs were added into the cell culture. After 24 h incubation, 20 mL of MTT solution in phosphate buffered saline (PBS) was added to each well and incubated for an additional 4 h. The cell culture was discarded afterwards with 150 mL dimethyl sulfoxide (DMSO) added to each well. We then incubated the plate at 37 °C for 5 min and shocked it for another 10 min at room temperature to allow complete dissolve of formazan. Finally, the absorbance at 570 nm of each well was measured by a microplate reader (Model 680 Bio-RAD) to determine the relative cell viability.

Characterization

Fourier transform infrared (FT-IR) spectra were recorded on a NICOLET-6700 FTIR spectrometer. Thermogravimetric analysis (TGA) was carried out on a 2960 SDT TA instruments with a heating rate of 10 °C min^{-1} from room temperature to 800 °C under a nitrogen atmosphere. Transmission electron micrographs were taken with a FEI TecnaiG220 (TEM) operated at an accelerating voltage of 200 kV. XRD (PANalytical Company, X'PERT PRO MPD, Cu Ka, $\lambda = 1.5406$ Å, X'Celerator) was used to determine the crystal structure of the pristine magnetic NPs. Fluorescent emission spectra were measured with excitation light of 294 nm wavelength in a PerkinElmer Ls-50B. A vibrating-sample magnetometer (VSM-7407, Lakeshore, USA) was used at room temperature to measure the magnetic properties of Fe_3O_4 and magnetic composite NPs.

Results and discussion

Synthesis of Fe_3O_4@SiO_2–BCBD

The immobilization of the macro-RAFT agent (Z–C(=S)–S–R), where carbazole was used as the Z group and a benzyl group tethered on the Fe_3O_4@SiO_2 NPs was used as the R group,[18] is the key step in whole process. With such grafted RAFT agent, dense polymer shells with tunable thickness can be easily

grafted on to the surfaces of Fe_3O_4@SiO_2 NPs with a controlled behavior *via* SI-RAFT polymerization. As for the synthesis of two-in-one magnetic fluorescent composites, the possible difficulty is the risk of quenching of the fluorophore on the surface of the NPs by the magnetic core and the mutual quenching of fluorescent molecules nearby in the case of a number of fluorescent molecules attached to the surface of the NPs. The whole process is shown in Scheme 1. Firstly, a certain thickness of silica colloids embedded with superparamagnetic Fe_3O_4 NPs was synthesized by a modified Stöber process. The magnetic NPs averaging about 9 nm of diameter and stabilized with citric acid in deionized water were used as the magnetic component of the composites. Secondly, Fe_3O_4@SiO_2 NPs were modified with (*p*-chloromethyl)phenyl trimethoxysilane to obtain the Fe_3O_4@SiO_2–Cl NPs. Finally, Fe_3O_4@SiO_2–BCBD NPs with fluorescent RAFT agent BCBD moieties were synthesized on the surface of Fe_3O_4@SiO_2 NPs by the reaction of sodium carbazole-9-carbodithioic acid and Fe_3O_4@SiO_2–Cl. Fig. 1(a–c) shows the UV-vis spectra of BCBD, NPs of Fe_3O_4@SiO_2 and Fe_3O_4@SiO_2–BCBD in DMF. The Fe_3O_4@SiO_2–BCBD suspension showed absorptions at 286 and 315 nm due to the phenyl rings and carbazole groups and the absorption at 365 nm was ascribed to the thiocarbonyl groups, which is similar to the absorbance of free BCBD. The fluorescence spectrum of Fe_3O_4@SiO_2–BCBD NPs in Fig. 1(d) showing peaks at 345 and 361 nm, typical peaks of the carbazole group, also proves the successful immobilization of BCBD on the surface of NPs.

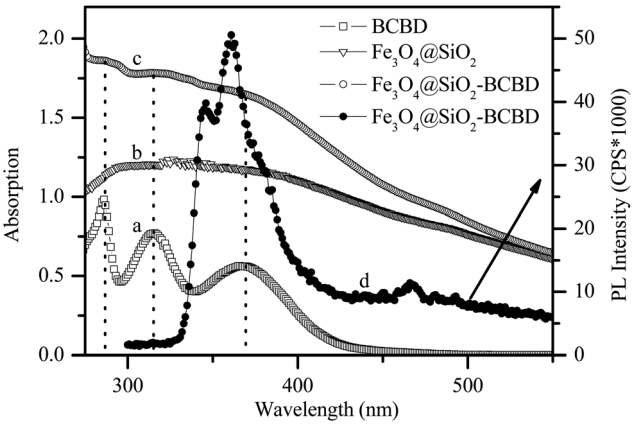

Fig. 1 UV-vis spectra of BCBD (a), NPs of Fe_3O_4@SiO_2 (b) and Fe_3O_4@SiO_2–BCBD (c) and fluorescence spectrum of Fe_3O_4@SiO_2–BCBD NPs (d) in DMF.

Synthesis of fluorescent monomer M_{HB}

M_{HB} was synthesized for the first time in our group by a convenient procedure as illustrated in Scheme 2. 1,2-Diaminobenzene reacts with 2-naphthoic acid with the aid of polyphosphoric acid to give the intermediate denoted as VNBI, which was used to react with 4-(chloromethyl)styrene by potassium carbonate catalysis to obtain the final product, the fluorescent monomer M_{HB}. The identity of the product was confirmed by ^{1}H NMR as shown in Fig. 2. Additional peaks at chemical shifts of 5.21, 5.73, 5.81 and 6.65 ppm in Fig. 2(b) compared to Fig. 2(a), arising from 4-(chloromethyl)styrene, appeared verifying the successful synthesis. The properties of M_{HB} were investigated; Fig. 3 shows the UV-vis spectrum (a) and excitation and emission fluorescence spectra (b) of M_{HB} in DMF. As Fig. 3(a) shows, M_{HB} has two absorption peaks at about 280 and 306 nm. Fluorescence spectra (Fig. 3(b)) reveal that M_{HB}

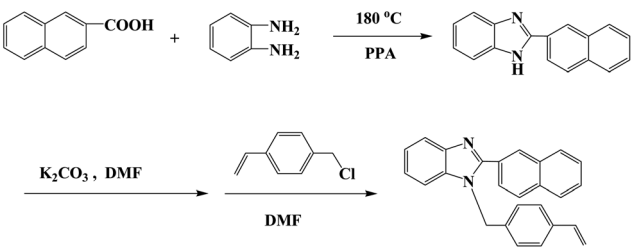

Scheme 2 Synthetic route to fluorescent monomer M_{HB}.

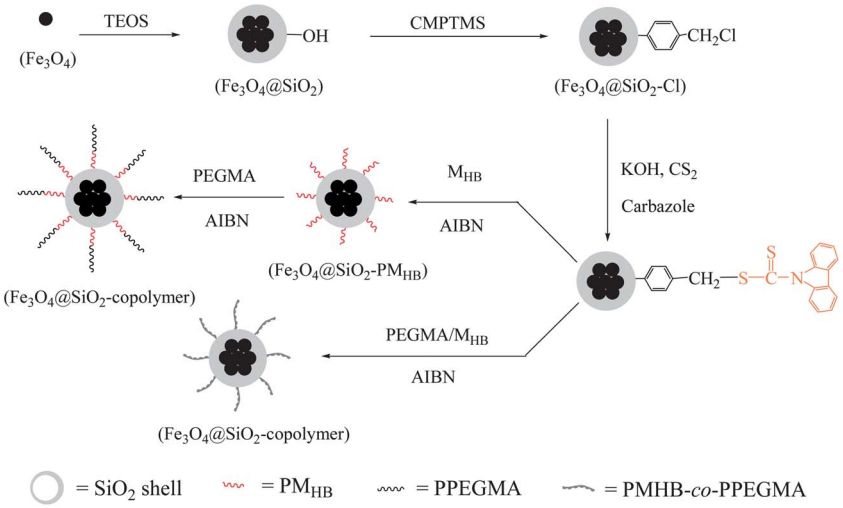

Scheme 1 Synthetic route of bifunctional NPs by SI-RAFT polymerization.

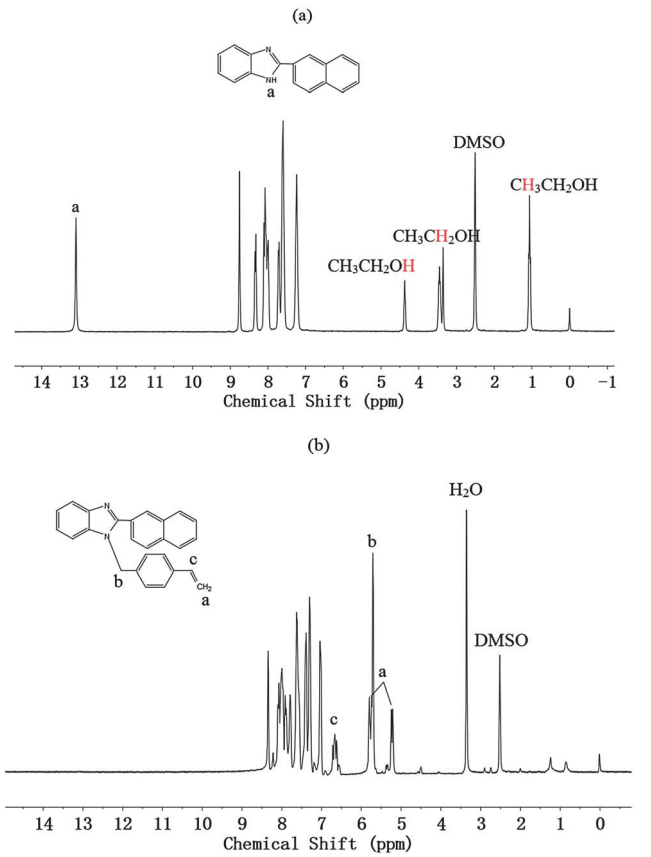

Fig. 2 ^{1}H NMR spectra of the intermediate VNBI (a) and M_{HB} (b).

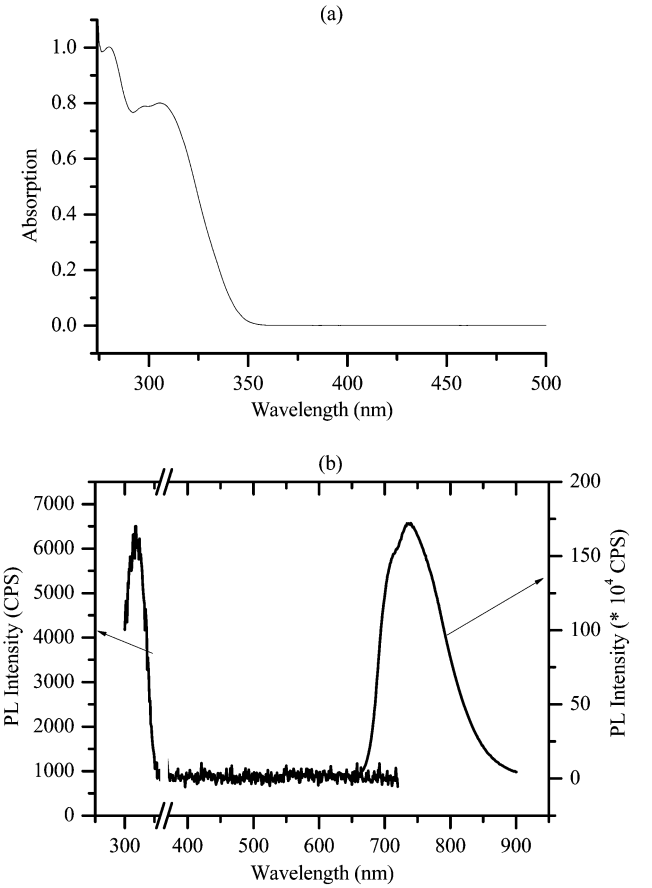

Fig. 3 UV-vis spectrum (a) and excitation and emission fluorescence spectra (b) of M_{HB} in DMF.

possesses the maximum excitation and emission at wavelength of 314 and 735 nm, respectively.

Grafting of M_{HB} on Fe_3O_4@SiO_2 NPs

By utilizing Fe_3O_4@SiO_2–BCBD NPs, M_{HB} can be easily grafted onto the surface of silica coated iron oxide. Herein we chose a hydrophilic and biocompatible monomer, PEGMA, to copolymerize or chain-extend after homopolymerization of M_{HB} to improve the hydrophilicity of the NPs as illustrated in Scheme 1. Fig. 4 shows the FT-IR spectra of the as-prepared NPs in different surface modification stages. Compared with Fig. 4(a), the peaks at 1092 cm^{-1} (Si–O–Si stretching) in Fig. 4(b)–(d) indicated successful coating of silica on the surface of iron oxide. The peak at 1730 cm^{-1}, which corresponds to the ester group originating from monomers in Fig. 4(d), confirmed that SI-RAFT polymerization was successfully performed. In order to further verify the copolymerization, the grafted polymer chain was cleaved from the NPs with 40 vol% hydrofluoric acid and was tested by ^{1}H NMR measurement, and the result is shown in Fig. 5. The peaks at chemical shifts from 6.5 to 7.5 ppm proved that the cleaved polymers consist of M_{HB} segment, indicating successful SI-RAFT copolymerization of M_{HB} and PEGMA. According to the peak area ratio of (c) to (b) in Fig. 5, it can be calculated that the molar ratio of PM_{HB}/PPEGMA is 2.1/100 in the grafted copolymer PM_{HB}-*co*-PPEGMA.

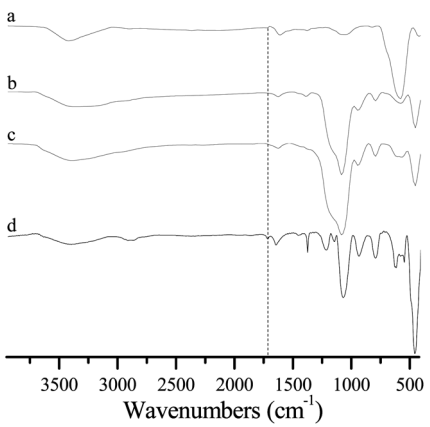

Fig. 4 FT-IR spectra of the as-prepared NPs of Fe_3O_4 (a), Fe_3O_4@SiO_2 (b), Fe_3O_4@SiO_2–BCBD (c) and Fe_3O_4@SiO_2@PM_{HB}-*co*-PPEGMA (d).

TEM images

Citric acid-stabilized Fe_3O_4 NPs with a diameter of 9 nm, as determined by TEM in Fig. 6(a), were prepared by a chemical coprecipitation method. The silica shell was then directly formed on the surfaces of Fe_3O_4 NPs through hydrolysis of TEOS in a mixture of ethanol, water and ammonia at 30 °C for

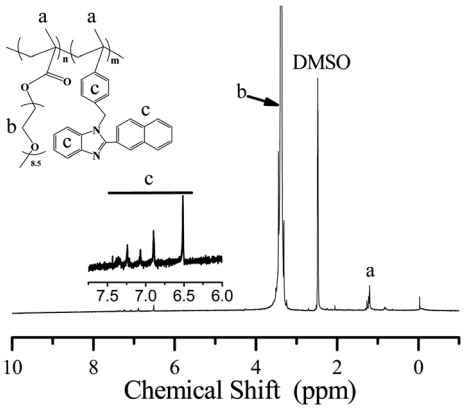

Fig. 5 ^{1}H NMR spectra of copolymer of M_{HB} with $PEGMA_{475}$ etched from Fe_3O_4@SiO_2@PM_{HB}-*co*-PPEGMA NPs.

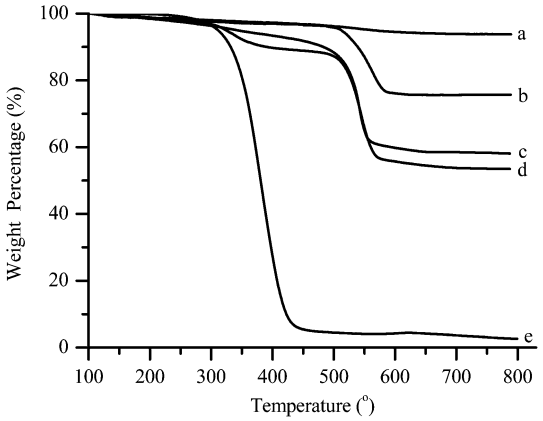

Fig. 7 TGA curves of the as-prepared NPs of Fe_3O_4@SiO_2 (a), Fe_3O_4@SiO_2–BCBD (b), Fe_3O_4@SiO_2@PM_{HB}-*co*-PPEGMA (c and d) and PM_{HB}-*co*-PPEGMA (e). $[PEGMA_{475}]_0/[M_{HB}]_0$ = 300 : 120, 300 : 30 for (c) and (d), respectively, t = 48 h.

24 h. As can be seen in Fig. 6(b), the diameter of the obtained hybrid NPs was about 150 nm after the Fe_3O_4 NPs were embedded. After the SI-RAFT polymerization, in Fig. 6(c), the Fe_3O_4@SiO_2 NPs were surrounded by the PM_{HB}-*co*-PPEGMA chains. The inset in Fig. 6(c) is a picture of Fe_3O_4@SiO_2@PM_{HB}-*co*-PPEGMA NPs dispersed in a mixed solvent of water and dichloromethane; the NPs were concentrated in the water fraction, indicating good hydrophilicity of the as-prepared Fe_3O_4@SiO_2@PM_{HB}-*co*-PPEGMA NPs.

TGA analysis

Fig. 7 shows the weight loss of NPs at various stages of surface modification at 800 °C. In Fig. 7(b), there is a significant weight loss around 550 °C caused by the decomposition of the organic components of Fe_3O_4@SiO_2–BCBD NPs, indicating the successful grafting of the BCBD RAFT agent. There exists an even bigger loss of weight around 550 °C in Fig. 7(c) and (d), proving the grafting of copolymers on the Fe_3O_4@SiO_2 surface, and the weight loss at around 330 °C in Fig. 7(c) and (d) is caused by the decomposition of the grafted copolymers, which is proved by the TGA curve of PM_{HB}-*co*-PPEGMA in Fig. 7(e).

XRD analysis

To confirm the structure of magnetic NPs and the successful embedding by SiO_2 and copolymers, the pure Fe_3O_4 NPs and the hybrid NPs were characterized by XRD. Fig. 8(a) shows the XRD pattern of Fe_3O_4 NPs, which indicates a highly crystalline cubic spinel structure. The reflection peak positions and relative intensities of Fe_3O_4 NPs agree well with the X-ray diffraction data cards (JCPDS, Joint Committee on Powder Diffraction Standards, no. 86-1354) according to which standard Fe_3O_4

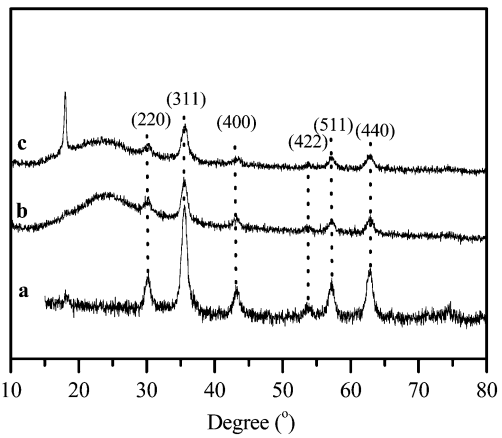

Fig. 8 XRD spectra of superparamagnetic NPs of Fe_3O_4 (a), Fe_3O_4@SiO_2 (b) and Fe_3O_4@SiO_2@PM_{HB}-*co*-PPEGMA (c).

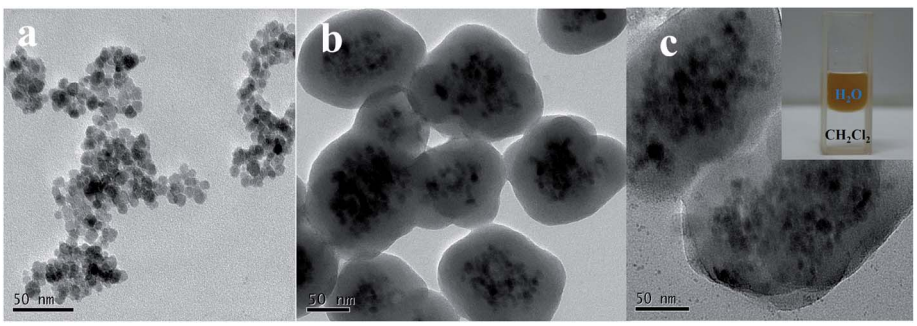

Fig. 6 TEM images of Fe_3O_4 (a) and Fe_3O_4@SiO_2 (b) and copolymer grafted Fe_3O_4@SiO_2@PM_{HB}-*co*-PPEGMA (c) NPs, inset in (c) is a photo of Fe_3O_4@SiO_2@PM_{HB}-*co*-PPEGMA NPs dispersed in a mixture of H_2O and CH_2Cl_2.

crystals with a spinel structure have six diffraction peaks: {2 2 0}, {3 1 1}, {4 0 0}, {4 2 2}, {5 1 1} and {4 4 0}. As shown in Fig. 8(b) and (c), the presented XRD pattern features six weak Bragg diffraction peaks at 20–80° 2θ, which can be indexed as {2 2 0}, {3 1 1}, {4 0 0}, {4 2 2}, {5 1 1} and {4 4 0} planes of pure Fe_3O_4 in a cubic phase. Therefore, it can be concluded that magnetic NPs dispersed in silica lattices are also of spinel structure. In addition, the broad peak appearing in the range from 18° to 28° indicates the existence of amorphous SiO_2 in the coating layer, and the sharp peak around 18° in Fig. 8(c) might be caused by the ordered alignment of the grafted polymers.

Properties of as-prepared NPs

The magnetic properties of the Fe_3O_4, Fe_3O_4@SiO_2 and Fe_3O_4@SiO_2@PM_{HB}-*co*-PPEGMA NPs were investigated using a VSM with fields up to 15 000 Oe. As shown in Fig. 9, hysteresis loops of the samples were registered at 300 K. These magnetic NPs are superparamagnetic at room temperature, as shown in Fig. 9(b), reaching a saturation moment of 13.0 emu g^{-1}. This saturation magnetization value, much lower than the saturation magnetization of the pure Fe_3O_4 NPs used for the preparation of these core–shell hybrid NPs (55.89 emu g^{-1}, Fig. 9(a)), can be explained by taking into account the diamagnetic contribution of the relatively thick silica shell surrounding the magnetic cores. Similarly, in Fig. 9(c), the saturation magnetization value of polymer grafted magnetic NPs decreased to 11.1 emu g^{-1}, which is lower than the pure Fe_3O_4 NPs as well as the Fe_3O_4@SiO_2 NPs for the same reason. However, these results indicate that the as-prepared NPs are suitable for magnetic guiding and imaging. In addition, neither coercivity nor remanence were observed among the three magnetization curves (Fig. 9), indicating the superparamagnetic character of the as-prepared NPs at 300 K. The inset in Fig. 9 is a photo of Fe_3O_4@SiO_2@PM_{HB}-*co*-PPEGMA NPs dispersed in DMF before and after exposure to a magnetic field. The fluorescent-magnetic hybrid NPs were completely separated from the solution within minutes but redispersed very well with a slight agitation when the external magnetic field was removed. This suggests that these magnetic silica coated NPs have good dispersibility and high sensitivity to the magnetic field, which are two important factors for bio-applications.

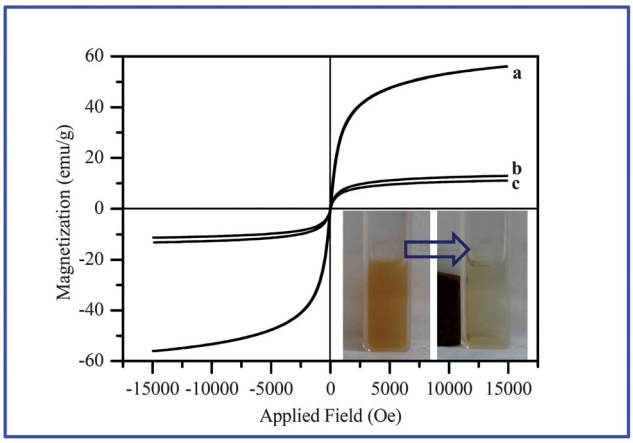

Fig. 9 Magnetic hysteresis loops at 300 K for the obtained NPs of (a) Fe_3O_4, (b) Fe_3O_4@SiO_2, (c) Fe_3O_4@SiO_2@PM_{HB}-*co*-PPEGMA with core–shell structures. The inset are photos of a copolymer grafted NPs dispersed in H_2O before (left) and after (right) magnetic separation.

Fluorescence

M_{HB} emits fluorescence at the wavelength of 750 nm in the NIR range when excited by a light at a wavelength of 315 nm in DMF. Fig. 10 shows the fluorescence spectra of Fe_3O_4@SiO_2@PM_{HB}-*co*-PPEGMA NPs with different feed ratios of PEGMA and M_{HB}. It is obvious that the fluorescence intensity can be easily adjusted by changing the $[PEGMA_{475}]_0/[M_{HB}]_0$ value. It can be seen that NPs with $[PEGMA_{475}]_0/[M_{HB}]_0 = 300/120$ (Fig. 10(a)) have higher fluorescence intensity than $[PEGMA_{475}]_0/[M_{HB}]_0 = 300/30$ (Fig. 10(b)). This is probably because polymerization with $[PEGMA_{475}]_0/[M_{HB}]_0 = 300/120$ leads to a high concentration of M_{HB} unit in the final NPs.

Another PEGMA with molecular weight of 1100 g mol^{-1} (denoted as $PEGMA_{1100}$) was also taken to copolymerize with

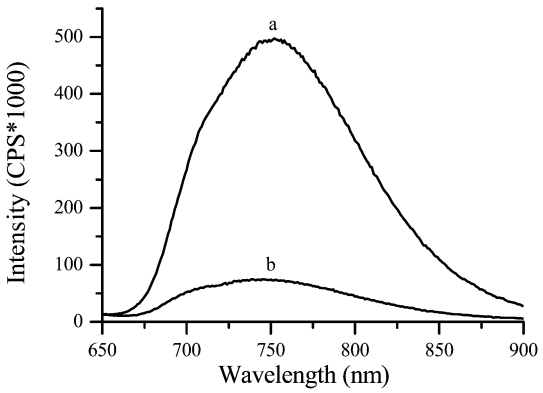

Fig. 10 Fluorescence spectra of NPs modified by copolymerization of M_{HB} and $PEGMA_{475}$ on the surface ($[PEGMA_{475}]_0/[M_{HB}]_0 = 300 : 120$, $300 : 30$ for (a) and (b), respectively) in DMF with maximum intensity; $t = 48$ h.

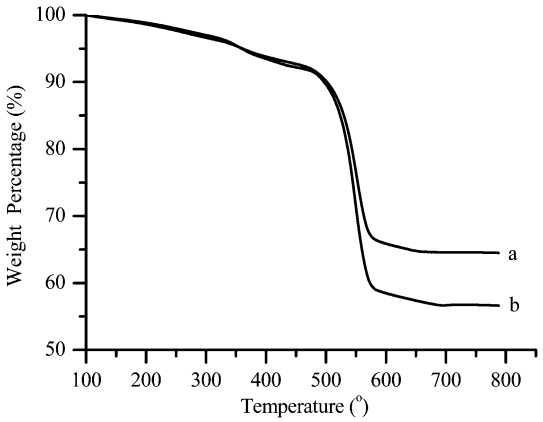

Fig. 11 TGA curves of the as-prepared NPs modified by copolymerization of M_{HB} and $PEGMA_{1100}$ on the surface ($[PEGMA_{1100}]_0/[M_{HB}]_0 = 120 : 30$, $142.5 : 7.5$ for (a) and (b), respectively); $t = 48$ h.

M_{HB} to investigate the fluorescence properties of the NPs. Fig. 11 shows the TGA curves of the copolymer grafted NPs. NPs with $[PEGMA_{1100}]_0/[M_{HB}]_0 = 120/30$ have a lower weight loss than $[PEGMA_{1100}]_0/[M_{HB}]_0 = 142.5/7.5$. The corresponding fluorescence spectra of the NPs are illustrated in Fig. 12. Contrary to the case of copolymerization of $PEGMA_{475}$ and M_{HB}, NPs with higher $[M_{HB}]_0/[PEGMA_{1100}]_0$ (30/120) exhibit lower fluorescence intensity than $[M_{HB}]_0/[PEGMA_{1100}]_0 = 7.5/142.5$. We attribute this to the differing reactivity ratios of $PEGMA_{1100}$ with M_{HB} compared to $PEGMA_{475}$ with M_{HB};[48] accordingly, the M_{HB} units are closer to each other and self-bleaching is more serious.

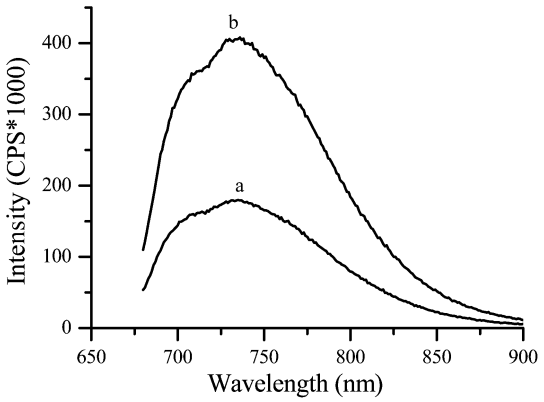

Fig. 12 Fluorescence spectra of NPs modified by copolymerization of M_{HB} and $PEGMA_{1100}$ on the surface ($[PEGMA_{1100}]_0/[M_{HB}]_0 = 120/30$, 142.5/7.5 for (a) and (b), respectively) in DMF with maximum intensity; $t = 48$ h.

The sequence of the polymers grafted on the surface of $Fe_3O_4@SiO_2$ could be easily controlled by feed orders. Besides random copolymers of M_{HB} with $PEGMA_{475}$, the homopolymer of M_{HB} and the block copolymer obtained by further chain-extension with $PEGMA_{475}$ after homopolymerization *via* SI-RAFT technique were also bound to the surface of the NPs. The fluorescence intensities of these NPs in DMF were investigated as shown in Fig. 13(a)–(c). All NPs showed maximum fluorescence intensity at a concentration of *ca.*125 μg mL^{-1} in DMF. The PM_{HB} homopolymer grafted NPs (Fig. 13(b)) exhibited higher intensity than copolymer grafted ones (Fig. 13(a)) due to higher M_{HB} concentration. The intensity for block copolymer grafted NPs (Fig. 13(c)) after chain-extension was also lower than for homopolymer grafted ones. This is probably caused by steric hindrance arising from the PPEGMA segments; as a consequence, the PM_{HB} chains are confined in smaller space and closer to each other giving rise to more self-bleaching. Aided by the silica shell and PPEGMA chains, the NPs also possess comparative stability when dispersed in water. The fluorescence properties of the suspensions in water were also recorded, and the results are listed in Fig. 13(d)–(f). Compared to Fig. 13(a)–(c), all the fluorescence intensities are reduced because of relatively poor dispersity of the NPs in water. However, the magnitudes of reduction of the NPs with PPEGMA moieties (Fig. 13(d) and (f)) are smaller than the homopolymer grafted ones (Fig. 13(e)), indicating an important role of PPEGMA in stabilizing the NPs and improving the dispersity. At a high concentration (200 μg mL^{-1}) the random copolymer grafted NPs (Fig. 13(d)) even shows the highest intensity among these three kinds of NPs. This is because M_{HB} unit is well

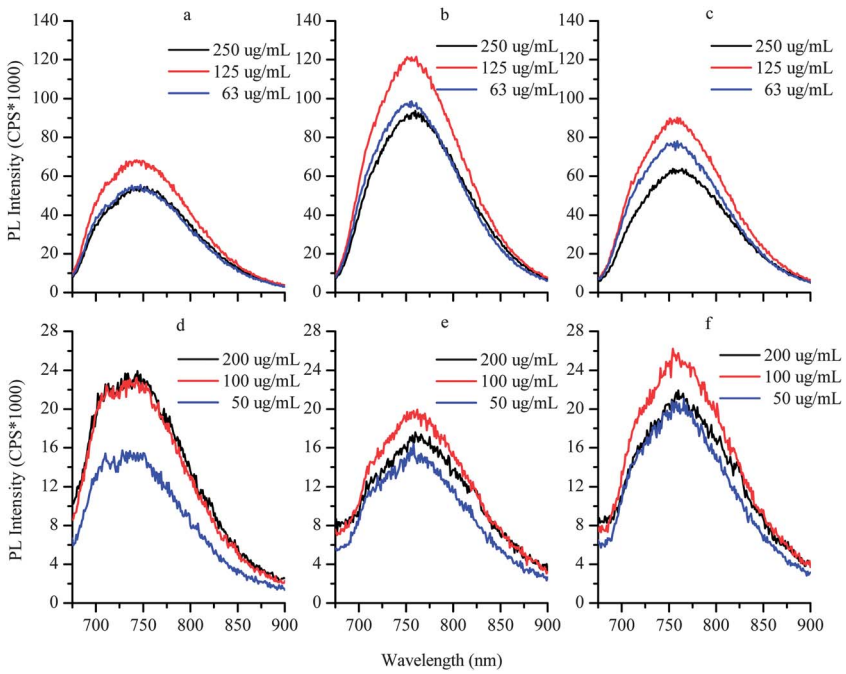

Fig. 13 Fluorescence spectra of NPs modified by (a and d) copolymerization of M_{HB} and $PEGMA_{475}$ ($[PEGMA_{475}]_0/[M_{HB}]_0/[AIBN]_0 = 300/30/1$, $Fe_3O_4@SiO_2$–BCBD = 50 mg), (b and e) homopolymerization of M_{HB} ($[M_{HB}]_0/[AIBN]_0 = 120/1$, $Fe_3O_4@SiO_2$–BCBD = 50 mg) and (c and f) block polymerization by chain-extension of $PEGMA_{475}$ ($[PEGMA_{475}]_0/[AIBN]_0 = 300/1$, $Fe_3O_4@SiO_2@PM_{HB}$ = 50 mg) on the surface in DMF (a–c) and in water (d–f) with different concentrations; $t = 24$ h.

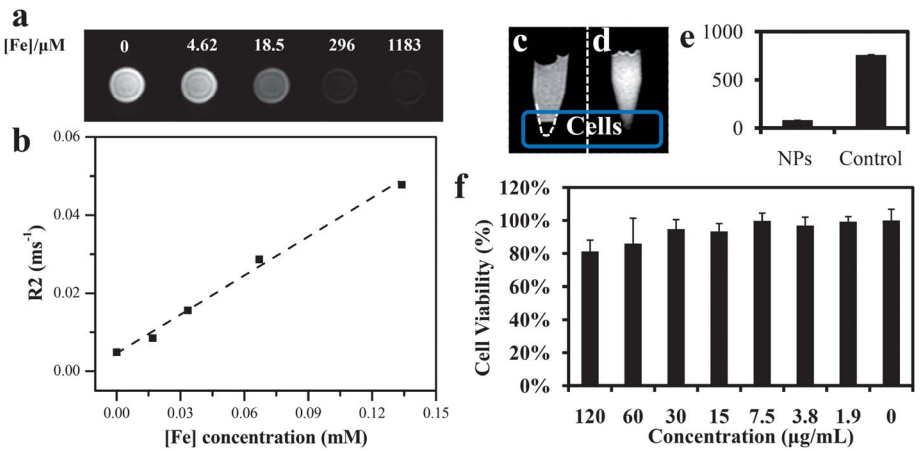

Fig. 14 MR imaging and cytotoxicity of Fe_3O_4@SiO_2@PM_{HB}-*co*-PPEGMA NPs. (a) T_2-weighed MR images (3.0 T; TR, 2000.00 ms; TE, 12.9 ms) of the Fe_3O_4@SiO_2@PM_{HB}-*co*-PPEGMA NPs. The iron concentration from left to right is 0, 4.62, 18.5, 295.8 and 1183 μmol L^{-1}, respectively. (b) The T_2 relaxation rates (r_2) of Fe_3O_4@SiO_2@PM_{HB}-*co*-PPEGMA NPs at different Fe concentrations. (c and d) *In vitro* T_2-weighed MR images of (c) the Fe_3O_4@SiO_2@PM_{HB}-*co*-PPEGMA NPs incubated with HeLa cells and (d) untreated cells; (e) shows the corresponding T_2 MR signal values, the Fe concentration incubated with cells being 10 μg L^{-1}. (f) Relative cell viability data of HeLa cells incubated with a series of iron concentrations of Fe_3O_4@SiO_2@PM_{HB}-*co*-PPEGMA NPs measured by the MTT cell viability assay; the incubation time was 24 h.

dispersed in a random order, indicating a suitable form for construction of such bifunctional NPs.

MR imaging and cytotoxicity

To validate the contrasting capacity of the hydrophilic Fe_3O_4@SiO_2@PM_{HB}-*co*-PPEGMA samples in contrasting MR images, we collected MR images at 3.0 T on an Artoscan Imager, commonly used for clinical investigation of diseases in articulations. MR images of the sample with different concentrations (0, 4.62, 18.5, 296 and 1183 μmol L^{-1}) were taken as shown in Fig. 14(a). As the iron concentration increased, the images became darker, showing a high transverse reflexivity (r_2) of 332.6 mM^{-1} s^{-1} (Fig. 14(b)) indicating effective T_2 contrast action of the as-prepared NPs. In addition, *in vitro* MR images of Fe_3O_4@SiO_2@PM_{HB}-*co*-PPEGMA incubated with HeLa cells are also shown in Fig. 14(c)–(e). The obvious darkening effect in Fig. 14(c) at the bottom of the tube reveals a good MRI contrast action of Fe_3O_4@SiO_2@PM_{HB}-*co*-PPEGMA for cell labeling. The corresponding T_2 MR signal values are 77 and 752 for the NP incubated cells and the control ones (Fig. 14(d)), respectively, as given in Fig. 14(e). The cytotoxicity of the as-prepared NPs was also investigated as shown in Fig. 14(f); more than 80 percent of the cells survived even at an iron concentration of 120 μg L^{-1}, indicating low toxicity of the NPs.

Conclusions

A novel strategy to synthesize hydrophilic hybrid NPs with magnetism and NIR fluorescence was developed successfully *via* SI-RAFT polymerization of a polymerizable fluorescent monomer, which might give some guidance in further designing and fabricating such bifunctional or multifunctional materials. Herein, the fluorophore comes from a monomer, first synthesized in our group, which is capable of emitting NIR fluorescence under UV irradiation. This new monomer was employed to perform homopolymerization, random and block copolymerization with a water-soluble monomer PEGMA on the surface of silica coated iron oxides. The as-prepared magnetic/NIR fluorescent NPs were used as an effective imaging agent in enhancing the negative contrast in MRI technique. Unfortunately, the UV excitation restricts its application in *in vitro* or *in vivo* detection because of the nature of the low penetration, high absorption and damage of UV light to cells and tissues. However, due to the development of modern techniques such as the recently demonstrated two-photon technique, this problem might be fixed in the near future.

Acknowledgements

The financial support from the National Natural Science Foundation of China (no. 21174096, 21274100 and 21234005), the Specialized Research Fund for the Doctoral Program of Higher Education (no. 20103201110005), the Project of International Cooperation of the Ministry of Science and Technology of China (no. 2011DFA50530), and the Project Funded by the Priority Academic Program Development of Jiangsu Higher Education Institutions (PAPD) is gratefully acknowledged.

References

1 J. Won, M. Kim, Y. Yi, Y. H. Kim, N. Jung and T. K. Kim, *Science*, 2005, **309**, 121–125.
2 V. Badilita, R. Ch. Meier, N. Spengler, U. Wallrabe, M. Utz and J. G. Korvink, *Soft Matter*, 2012, **8**, 10583–10597.
3 Y. Huh, Y. Jun, H. Song, S. Kim, J. Choi, J. Lee, S. Yoon, K. Kim, J. Shin, J. Suh and J. Cheon, *J. Am. Chem. Soc.*, 2005, **127**, 12387–12391.
4 C. Corot, P. Robert and M. Port, *Adv. Drug Delivery Rev.*, 2006, **58**, 1471–1504.

5 X. Shi, S. H. Wang, S. D. Swanson, S. Ge, Z. Cao, M. E. Van Antwerp, K. J. Landmark and J. R. Baker, *Adv. Mater.*, 2008, **20**, 1671–1678.
6 E. S. M. Lee, B. Shuter, J. Chan, M. S. K. Chong, J. Ding, S. H. Teoh, O. Beuf, A. Briguet, K. C. Tam, A. Choolani and S. C. Wang, *Biomaterials*, 2010, **31**, 3296–3306.
7 I. Safarik, K. Pospiskova, K. Horska and M. Safarikova, *Soft Matter*, 2012, **8**, 5407–5413.
8 P. Tartaj, M. P. Morales, T. Gonzalez-Carreño, S. Veintemillas-Verdaguer and C. J. Serna, *Adv. Mater.*, 2011, **23**, 5243–5249.
9 K. G. Neoh and E. T. Kang, *Soft Matter*, 2012, **8**, 2057–2069.
10 N. Ahmed, M. Michelin-Jamois, H. Fessi and A. Elaissari, *Soft Matter*, 2012, **8**, 2554–2564.
11 F. Yang, Y. Li, Z. Chen, Y. Zhang, J. Wu and N. Gu, *Biomaterials*, 2009, **30**, 3882–3890.
12 L. L. Zhao, L. J. Zhu, Q. Wang, J. L. Li, C. L. Zhang, J. G. Liu, X. Z. Qu, G. L. He, Y. F. Lu and Z. Z. Yang, *Soft Matter*, 2011, **7**, 6144–6150.
13 S. A. Corr, S. J. Byrne, R. Tekoriute, C. J. Meledandri, D. F. Brougham, M. Lynch, C. Kerskens, L. O'Dwyer and Y. K. Gun'ko, *J. Am. Chem. Soc.*, 2008, **130**, 4214–4215.
14 S. A. Corr, Y. P. Rakovich and Y. K. Gun'ko, *Nanoscale Res. Lett.*, 2008, **3**, 87–104.
15 L. Zhou, J. Yuan, W. Yuan, M. Zhou, S. Wu, Z. Li, X. Xing and D. Shen, *Mater. Lett.*, 2009, **63**, 1567–1570.
16 N. Hirata, K. Tanabe, A. Narita, K. Tanaka, K. Naka, Y. Chujo and S. Nishimoto, *Bioorg. Med. Chem.*, 2009, **17**, 3775–3781.
17 H. Skaat and S. Marge, *Biochem. Biophys. Res. Commun.*, 2009, **386**, 645–649.
18 Q. Li, L. F. Zhang, L. J. Bai, Z. B. Zhang, J. Zhu, N. C. Zhou, Z. P. Cheng and X. L. Zhu, *Soft Matter*, 2011, **7**, 6958–6966.
19 J. L. Liu, W. W. He, L. F. Zhang, Z. B. Zhang, J. Zhu, Z. P. Cheng and X. L. Zhu, *Langmuir*, 2011, **27**, 12684–12692.
20 Y. S. Lin, S. H. Wu, Y. Hung, Y. H. Chou, C. Chang, M. L. Lin, C. P. Tsai and C. Y. Mou, *Chem. Mater.*, 2006, **18**, 5170–5172.
21 S. C. Wuang, K. G. Neoh, E. T. Kang, D. W. Pack and D. E. Leckband, *Biomaterials*, 2008, **29**, 2270–2279.
22 S. Dubus, J. F. Gravel, B. L. Drogoff, P. Nobert, T. Veres and D. Boudreau, *Anal. Chem.*, 2006, **78**, 4457–4464.
23 D. Wang, J. He, N. Rosenzweig and Z. Rosenzweig, *Nano Lett.*, 2004, **4**, 409–413.
24 A. K. Gupta and M. Gupta, *Biomaterials*, 2005, **26**, 3995–4021.
25 N. Gaponik, I. L. Radtchenko, G. B. Sukhorukov and A. L. Rogach, *Langmuir*, 2004, **20**, 1449–1452.
26 L. Josephson, M. F. Kircher, U. Mahmood, Y. Tang and R. Weissleder, *Bioconjugate Chem.*, 2002, **13**, 554–560.
27 J. Zhou, Y. Sun, X. Du, L. Xiong, H. Hu and F. Li, *Biomaterials*, 2010, **31**, 3287–3295.
28 P. A. Jarzyna, T. Skajaa, A. Gianella, D. P. Cormode, D. D. Samber, S. D. Dickson, W. Chen, A. Griffioen, Z. Fayad and W. Mulder, *Biomaterials*, 2009, **30**, 6947–6954.
29 C. M. Lee, D. R. Jang, J. Kim, S. J. Cheong, E. M. Kim, M. H. Jeong, S. Kim, D. Kim, S. Lim, M. Sohn, Y. Jeong and H. Jeong, *Bioconjugate Chem.*, 2011, **22**, 186–192.
30 L. Cheng, K. Yang, Y. Li, J. Chen, C. Wang, M. Shao, S. Lee and Z. Liu, *Angew. Chem., Int. Ed.*, 2011, **50**, 7385–7390.
31 H. Xu, L. Cheng, C. Wang, X. Ma, Y. Li and Z. Liu, *Biomaterials*, 2011, **32**, 9364–9373.
32 J. V. Frangioni, *Curr. Opin. Chem. Biol.*, 2003, **7**, 626–634.
33 P. Sharma, S. Brown, G. Walter, S. Santra and B. Moudgil, *Adv. Colloid Interface Sci.*, 2006, **126**, 471–485.
34 C. H. Tung, *Biopolymers*, 2004, **76**, 391–403.
35 A. Zaheer, R. E. Lenkinskl, A. Mahmood, A. C. Jones, L. C. Cantley and J. V. Frangioni, *Nat. Biotechnol.*, 2001, **19**, 1148–1154.
36 Y. T. Lim, S. Kim, A. Nakayama, N. E. Stott, M. G. Bawendi and J. V. Frangioni, *Mol. Imaging*, 2003, **2**, 50–64.
37 I. L. Medintz, H. T. Uyeda, E. R. Goldman and H. Mattoussi, *Nat. Mater.*, 2005, **4**, 435–446.
38 L. Yuan, W. Y. Lin, K. B. Zheng, L. W. He and W. M. Huang, *Chem. Soc. Rev.*, 2012, **42**, 622–661.
39 L. Yuan, W. Y. Lin, Y. T. Yang and H. Chen, *J. Am. Chem. Soc.*, 2012, **134**, 1200–1211.
40 N. Karton-Lifshin, E. Segal, L. Omer, M. Portnoy, R. Satchi-Fainaro and D. Shabat, *J. Am. Chem. Soc.*, 2011, **133**, 10960–10965.
41 C. Thivierge, A. Loude and K. Burgess, *Macromolecules*, 2011, **44**, 4012–4015.
42 W. Yue, Y. Zhao, S. Shao, H. Tian, Z. Xie and Y. Geng, *J. Mater. Chem.*, 2009, **19**, 2199–2206.
43 A. Samanta, M. Vendrell, R. Das and Y. T. Chang, *Chem. Commun.*, 2010, **46**, 7406–7408.
44 G. Qian, B. Dai, M. Luo, D. Yu, J. Zhan, Z. Zhang, D. Ma and Z. Wang, *Chem. Mater.*, 2008, **20**, 6208–6216.
45 J. Pauli, R. Brehm, M. Spieles, W. A. Kaiser, I. Hilger and U. Resch-Genger, *J Fluoresc.*, 2010, **20**, 681–693.
46 X. Peng, F. Song, E. Lu, Y. Wang, W. Zhou, J. Fan and Y. Gao, *J. Am. Chem. Soc.*, 2005, **127**, 4170–4171.
47 C. Z. Li and B. C. Benicewicz, *Macromolecules*, 2005, **38**, 5929–5936.
48 S. Huijser, G. D. Mooiweer, R. van der Hofstad, B. B. P. Staal, J. Feenstra, A. M. van Herk, C. E. Koning and R. Duchateau, *Macromolecules*, 2012, **45**, 4500–4510.